archaeometry

Archaeometry **61**, 2 (2019) 459–469 doi: 10.1111/arcm.12419

RAMAN BINARY MAPPING OF IRON AGE OSTRACON IN AN UNKNOWN MATERIAL COMPOSITION AND HIGH-FLUORESCENCE SETTING—A PROOF OF CONCEPT*

A. SHAUS† and B. SOBER

Department of Applied Mathematics, Tel Aviv University, Ramat Aviv, Tel Aviv 6997801, Israel

O. TZANG, Z. IOFFE and O. CHESHNOVSKY

Department of Chemical Physics, Tel Aviv University, P.O. Box 39040, Tel Aviv 6997801, Israel

I. FINKELSTEIN

Department of Archaeology and Ancient Near Eastern Cultures, Tel Aviv University, Ramat Aviv, Tel Aviv 6997801, Israel

and E. PIASETZKY

Department of Particle Physics, Tel Aviv University, P.O. Box 39040, Tel Aviv 6997801, Israel

The textual evidence from ancient Judah is mainly limited to ostraca, ink-on-clay inscriptions. Their facsimiles (binary depictions) are indispensable for further analysis. Previous attempts at mechanizing the creation of facsimiles have been problematic. Here, we present a proof of concept of objective binary image acquisition, via Raman mapping. Our method is based on a new peak detection transform, handling the challenging fluorescence of the clay, and circumventing preparatory ink composition analysis. A sequence of binary mappings (signifying the peaks) is created for each wavelength; their legibility reflects the prominence of Raman lines. Applied to a biblical-period ostracon, the method exhibits high statistical significance.

KEYWORDS: RAMAN MAPPING, BIBLICAL ARCHAEOLOGY, OSTRACON, FACSIMILE, HIGH FLUORESCENCE, PEAK TRANSFORM, IMPLICIT AND POSTERIOR COMPOSITION ANALYSIS

INTRODUCTION

The field of Iron Age epigraphy (the study of inscriptions and writing) is important for the domains of biblical archaeology, the history of ancient Israel and biblical studies. The most abundant texts that have come down to us from the First Temple period are *ostraca* inscriptions (clay potsherds inscribed in ink or incised). These are traditionally handled by experts, who study them by creating *manual facsimiles* (black and white—i.e., binary—depictions of the text), and who are potentially biased by their prior knowledge or inclinations (Shaus *et al*. 2010, 2012a). Such facsimiles may lead to inaccurate text transliterations, translations, palaeographical analysis and dating of the inscriptions, all of which influence archaeological and historical interpretations (Faigenbaum-Golovin *et al*. 2016).

Until now, multispectral techniques have been used in order to enhance the legibility of ostraca (Faigenbaum *et al*. 2012), with varying degrees of success. This technique produces improved

*Received 16 March 2016; accepted 3 July 2018
†Corresponding author: email ashaus@post.tau.ac.il

greyscale, rather than binary (black and white) images. Efforts to produce new facsimiles automatically, or to improve existing ones, have also been undertaken (Shaus *et al*. 2012b, 2013, 2016; Faigenbaum *et al*. 2013; Shaus and Turkel 2016, 2017). Unfortunately, these image processing and analysis methods, including techniques specifically tailored for ostraca, have often created problematic results.

In this paper, we aim to produce an alternative binarization procedure, based on Raman mapping. In the past, Raman spectroscopy techniques have been found to be valuable in several pottery-related domains: identification of pigments, analysis of mineralogical composition of ceramics and understanding of pottery production processes (for a survey of these, see Ricciardi 2008). To the best of our knowledge, our attempt to create a facsimile of an ostraca inscription based on Raman techniques is the first of its kind.

Until recently, research dealing with the ink composition of First Temple period ostraca has been scarce and inconclusive. A pioneering study of the ink of the ostraca corpus of Lachish (an ancient site in the Shephelah region; Lewis 1937, 1938) concluded that some 'brownish' ink was of mixed iron–carbon composition, while the commonplace, 'more eroded' ink was mainly carbon based; no details of the organic composition of the ink were provided. A short report on the ostraca from Arad (an ancient site in the Beer Sheba Valley; Gopher 1981) concluded that the ink was primarily, and perhaps exclusively, made of carbon material. A more recent study (Nir-El *et al*. 2015) that examined two inscriptions from Tel Malhata (also in the Beer Sheba Valley) via XRF showed traces of iron in the 'red' ink of an ostracon, but no noticeable traces of iron in the 'black' ink. The iron-based ink was very probably based on dark red ferric oxide, Fe_2O_3 (hematite). Subsequent XRF experiments performed by our team on additional Tel Malhata and Horvat 'Uza (another site in the Beer Sheba Valley) black ink ostraca revealed no traces of iron. The analysis could not explicitly identify carbon, since its characteristic X-ray energy is far below the detection threshold of the equipment used. The black ink is thus not iron-based, and it is presumably lampblack or soot. In addition, one cannot rule out the possibility that the composition of the organic ink was changed by post-depositional processes, resulting in humic acids.

Commonly, Raman mapping (or analysis) begins with identifying the Raman lines of the materials under investigation. Later, the indicative signals are combined in order to create a Raman mapping image. However, due to uncertainty and possible variability in ink and clay composition (even within a single ostracon), it is not feasible to follow this protocol in our case.

Instead of the regular approach, this paper proposes a proof of concept for an alternative mapping procedure, *circumventing the need for preliminary composition analysis*. Our method is based upon a peak detection transform, designed in a robust manner in order to overcome the problematic fluorescence induced by the clay medium. The transform translates each spectrum into a set of pronounced peaks (i.e., potential Raman lines). Subsequently, a series of binary mappings, corresponding to different Raman lines, is generated. These images exhibit the effect of certain Raman lines on the resulting foreground/background (ink/clay) separation. The Raman lines strongly characterizing ink but not clay (or vice versa) produce the most legible binarizations of the ostracon. The legibility is quantified by an automatic assessment procedure, choosing the most favourable Raman lines. The experiments showcasing this methodology exhibit extremely high statistical significance.

It will be stressed that this is a feasibility study for a new technology. At this stage, we have not conducted extensive comparisons with software-based image binarization algorithms (e.g., Shaus *et al*. 2012b, 2013). In addition, an already existing methodology of multispectral imaging of ostraca (see Faigenbaum *et al*. 2012) was not compared with the proposed technique, as the multispectral images are not binary.

EXPERIMENTAL

Preliminary Raman experiments

As a proof-of-concept step, several small-scale Raman spectral samplings of the ink (foreground) and clay (background) were undertaken. This was done using a home-built scanning confocal Raman microscope operating in reflection mode, with through-the-objective illumination from a fibre-coupled 532 solid-state green laser with an effective power on the samples of ~5 mW (for details, see Ioffe *et al*. 2008). The preliminary results demonstrated a potential for differentiating between ink and clay spectra, despite the high fluorescence of the sampled data.

The samples for this study were taken from an unpublished black ink Edomite ostracon (excavation registry number 36458; see Fig. 1). This inscription was found in the excavations of Horvat 'Uza, a late Iron Age (*c*.600 BCE) Judahite military outpost located in the Beer Sheba Valley, along with 38 other ostraca (Beit-Arieh 2007). Figure 2 shows examples of foreground and background spectra sampled from this ostracon. The figure exhibits the high fluorescence of the ostraca medium, present in both ink and clay samples. The resulting fluctuations can create false 'signals' that might mislead an attempted analysis of the spectra. In fact, these 'false signals' can be attributed to 'shot noise', which increases with the square root of the number of counts. Indeed, this increase can be seen in Figure 2 (i.e., the higher the graph, the larger is the local noise). Therefore, a detection of indicative peaks (e.g., at ~1600 cm^{-1}, corresponding to an organic substance containing aromatic rings, possibly humic acid or soot) is challenging and requires appropriate algorithmic machinery, described in the following subsection.

A series of small-scale experiments, aimed at measuring the effect of the laser on the ostracon's ink, were also carried out. These were meant to verify that the nominal mapping energy levels (i.e., the energy levels expected in our mapping device) are safe for this and other similar artefacts. It is worth mentioning that the experiments were performed on the ostracon itself and not on a model, since the exact composition of the ink and clay, as well as post-depositional processes that the ostraca commonly undergo, are difficult to reproduce. Our results demonstrate that the use of energy levels up to 12.6 times the nominal mapping energies does not produce any noticeable damage to the ostracon. Some damage was observed starting at energies 56.8 times the nominal level. It will be stressed that while performing a limited number of such experiments on

Figure 1 *The Edomite ostracon (ink-on-clay inscription) from Horvat 'Uza (excavation registry number 36458). [Colour figure can be viewed at wileyonlinelibrary.com]*

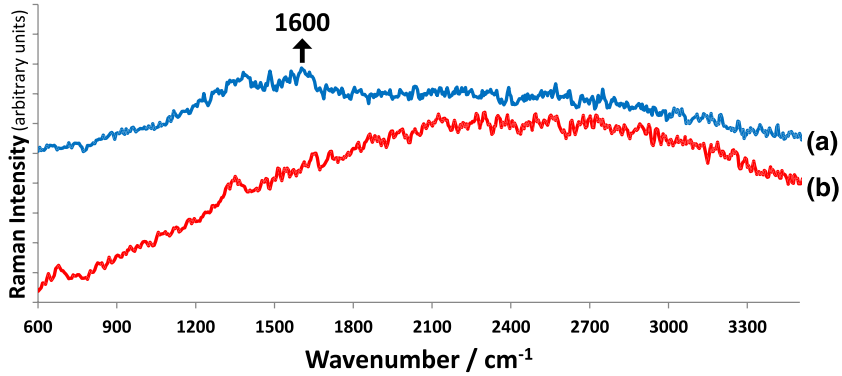

Figure 2 *Ink (a) versus clay (b) spectra, sampled from the Horvat 'Uza ostracon (registry number 36458), using a 532 nm laser. The arrow points to a peak indicative of ink at ~1600 cm^{-1}, corresponding to an organic substance containing aromatic rings, possibly humic acid or soot. A relatively high fluorescence can also be observed. [Colour figure can be viewed at wileyonlinelibrary.com]*

valuable ancient materials, we did not aim at establishing the exact energy level at which the damage begins to occur. For additional details regarding the experiments, such as power and exposure times, see the Appendix.

The peak detection transform

The purpose of the algorithm is to automatically extract the most pronounced peaks (potential Raman lines) from the noisy spectral data. At this stage, we prefer to have over-, rather than under-detection (at a subsequent stage, utilizing the macro-scale mappings based on the extracted peaks, the meaningful Raman lines will be identified).

The stages of the peak detection transform are as follows:

(1) For each element of the spectra S_w (representing the count at wavelength w), verify whether $S_w = \max\{S_u\}_{u=w-W}^{w+W}$; that is, S_w is the local maximum within a window of radius W. If not, ignore it.
(2) Calculate the heights of the remaining local maxima: $H_w = S_w - \min\{S_u\}_{u=w-W}^{w+W}$.
(3) Sort the resulting heights: $H_{w_1} \geq H_{w_2} \geq H_{w_3} \ldots$; choose the largest N heights, $H_{w_1}, H_{w_2}, \ldots H_{w_N}$. Their corresponding wavelengths are the detected peaks, $\{w_i\}_{i=1}^{N}$.

Remarks:

- The transform operates on the original wavelength scale, as sampled by our system and following its light dispersion model.
- W and N are predetermined parameters. In our setting, we used the values $W = 1$ nm and $N = 20$.
- We limit ourselves to spectra S_w such that $w > LaserWavelength + Const$, eliminating anti-Stokes and notch filter spectrum values.

It is worth mentioning that the ink-indicative peak at ~1600 cm^{-1}, which appears in Figure 2, was located with no human intervention via the peak detection transform. The spectra shown in Figure 2 are representative of several dozen additional experiments performed in similar settings. They showcase both the potential of distinguishing between clay and ink as well as the fluorescence challenges of the ostraca medium. Macro-scale experiments performed with an improved setting are described in the following subsections.

Mapping set-up

The experiments involved the use and adaptation of the home-built confocal Raman microscope (Tzang *et al*. 2011). In an attempt to reduce the high fluorescence stemming from the ceramics (as well as further minimizing the potential damage to the artefact), a shift to a laser with a longer wavelength was undertaken. Thus, an 8 mW solid state 671 nm CW laser was utilized in all further experiments. The confocal Raman microscope includes an optical system, a notch filter, a spectrograph and an auto-focus mechanism based on a digital camera coupled with a scanning table capable of 3D movements (see Fig. S1).

The typical mapping area was square-shaped, up to several millimetres wide (the largest mapping attempted was performed on an area of $0.5 \times 0.5\,\text{cm}^2$). The spatial ($XY$) resolution was chosen to be 30–60 μm^2, with a laser beam diameter of ~30 μm. Due to the curved and uneven surface of the pottery, an auto-focus procedure was carried out at each sampled pixel. Moreover, as the fluorescence and focal point of the surface varied rapidly, each pixel was sampled at 10 different Z-axis elevations. The spectrum acquisition speed (camera exposure time) was ~1 s.

The scanning procedure was as follows:

(1) Obtain a 4D spectral matrix $M[x, y, z, w]$, where (x, y) are the spatial coordinates (pixels), $z = z_1, \ldots, z_{10}$ stemming from the 10 different Z-axis elevations, and the w are the different wavelengths.
(2) Attain a 4D binary matrix $P[x, y, z, w]$, with each coordinate containing either 0 (False) or 1 (True), indicating whether a peak was found at wavelength w of spectra sampled at (x, y, z).
(3) For each wavelength λ, create a corresponding I_λ image: $I_\lambda[x, y] = \max_{z=z_1,\ldots,z_{10}} \{P[x, y, z, \lambda]\}$—that is, mark the pixel as True if at least one of its spectra contains a peak at wavelength λ; otherwise mark it as False (logical OR rule).
(4) Translate the I_λ image into a computer black-and-white image, with 1 = True and 0 = False values transformed, respectively, into 0 and 255 grey levels.
(5) *Optional*: post-processing of I_λ images. In our cases, we tried two configurations:
    (a) Application of the median filter (substituting a value of each pixel with a median value of pixels in a window centred on that pixel; we used a window size of 7×7 pixels), as well as unifying neighbouring images with respect to wavelength λ (five consecutive images unified for each λ in our case).
    (b) Application of the percentile filter (substituting a value of each pixel with a percentile value of pixels in a window centred on that pixel; we used a window size of 5×5 pixels and a percentile of 20%).
(6) The best images can be selected out of a few hundred I_λ images (or their post-processed counterparts), based on a simple visual inspection. Alternatively, automatic image selection can be applied based on measures such as the PC measure defined in Faigenbaum *et al*. (2012). In our experiment, the automatic selection yielded the same selection of optimal images as human observation.

RESULTS

Macro-scale mapping

The macro-scale mapping experiments focused on two different areas of the Horvat ʻUza ostracon. Several typical I_λ images for one of the scans can be seen in Figure 3, with black pixels indicating the existence of signal (i.e., the peak at λ). It can be observed that the resulting maps may be

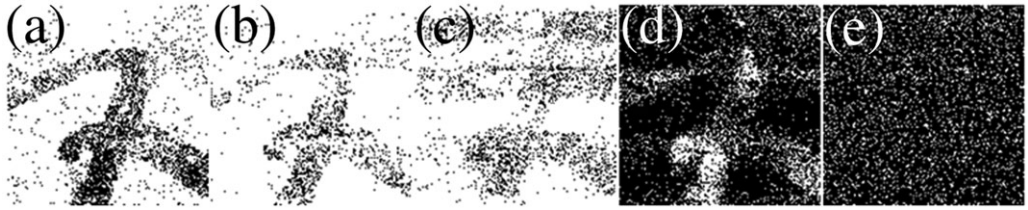

Figure 3 *Examples of different I_λ images, with black pixels indicating 'signal'; that is, a peak found by our methodology. (a) ~1460 cm^{-1}, an 'ink' signal; (b) ~1860 cm^{-1}, an 'ink' signal; (c) ~1580 cm^{-1}, an 'ink' signal; (d) ~1120 cm^{-1}, a 'clay' signal; (e) ~3920 cm^{-1}, typical white noise.*

dominated by signals stemming from the foreground (ink; see Figs 3 (a) – 3 (c)), the background (clay; see Fig. 3 (d)) or different kinds of noise (see Fig. 3 (e)). Evidently, in the case of a background signal, the map will result in a 'negative' image.

Representative fluorescent spectra of ink and clay are provided in Figure 4. Some Raman lines, characteristic for clay (e.g., ~1120 cm^{-1}) and ink (e.g., ~1470 cm^{-1}, ~1580 cm^{-1} and ~1860 cm^{-1}), were detected automatically by the peak detection transform, and are also marked. These peaks are not just mere fluorescence spikes but, rather, indicative Raman lines, producing the exceptionally non-random maps of Figure 3 (considering a certain amount of overlap between consecutive bins at the sampling level, the neighbouring 1460 cm^{-1} and 1470 cm^{-1} Raman lines cannot be distinguished).

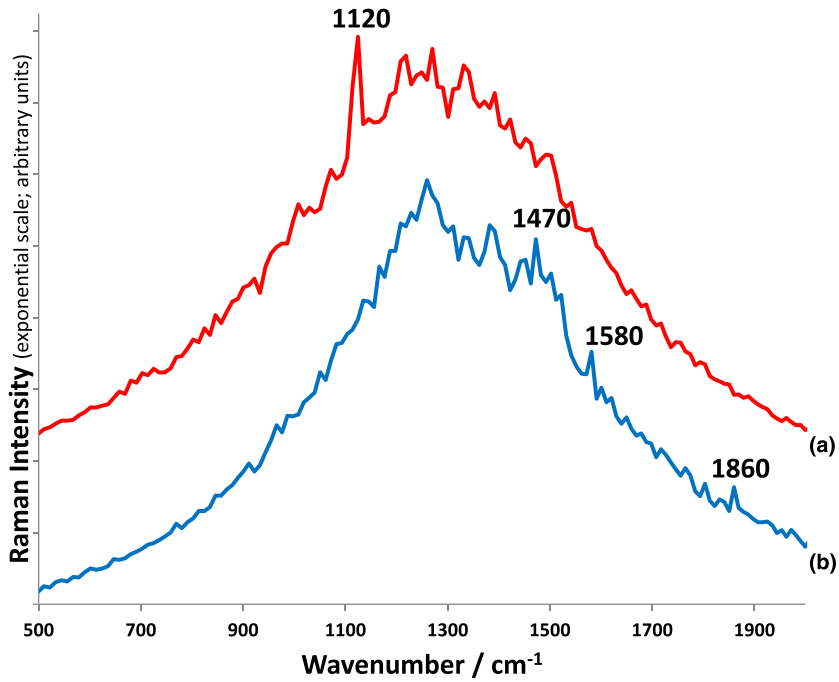

Figure 4 *Representative ink (a) and clay (b) spectra from the first mapping experiment, using a 671 nm laser. The indicative Raman lines for ink (~1470 cm^{-1}, ~1580 cm^{-1} and ~1860 cm^{-1}) and clay (~1120 cm^{-1}), marked on the spectra, were automatically identified by the peak detection transform. Note the exponential scale of the Y-axis, used in order to emphasize the results. [Colour figure can be viewed at wileyonlinelibrary.com]*

The best results of two scans, including the mapping areas, the I_λ images registered to the ostracon image and the I_λ images after different types of post-processing, can be seen in Figure 5. Note that our registrations are imperfect due to the ostracon's irregular geometry.

The results indicate that our macro-area mapping is plausible. Moreover, *the results are by no means random*, as no type of spectral noise can produce meaningful mappings. The demonstrative binarizations imply that the results possess extremely high statistical significance. Namely, the probability of obtaining I_λ image with similar (or better) correlation to the ostracon at random (i.e., the *p*-value) is estimated to be less than 10^{-30}.

Comparison with other analysis methods

In addition to our peak detection based analysis, the well-established principal component analysis (PCA, commonly used in Raman spectroscopy; e.g., Gierlinger *et al*. 2012) and the support vector machine (SVM; Cortes and Vapnik 1995) were also applied to the data, via the appropriate R language libraries (R Development Core Team 2008; Meyer *et al*. 2015). In order to run the SVM kernel, two training sets (ink and clay) of dimension $3 \times 3 \times 10$ were sampled prior to the experiment. In addition, several SVM kernels (linear, radial and polynomial with degrees 3, 5 and 7) were attempted. A comparison of the best PCA and SVM outcomes with our results can be seen in Figure 6.

It can be observed that, as expected, the PCA algorithm produced a greyscale image reminiscent of the regular digital image. The SVM produced a notable result, albeit based on a training procedure. The peak detection algorithm reported here seems superior to the other methods. In addition, as a by-product, our method allows for the detection of indicative Raman lines (see

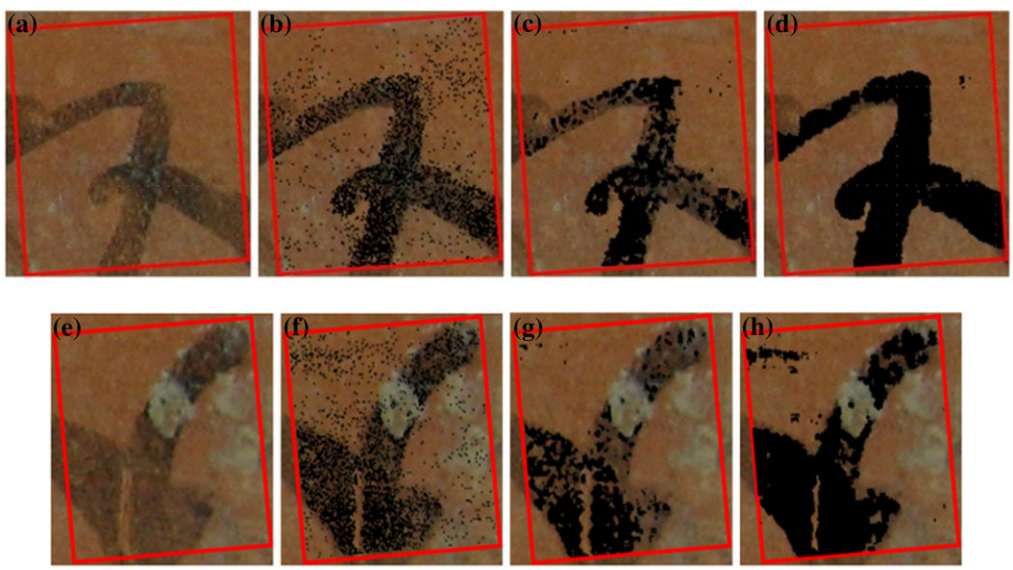

Figure 5 *The results of the first (a–d) and the second (e–h) mapping experiments: (a, e) photographs of the mapping area; (b, f) mapping results for ~1460 cm^{-1} overlaid; (c, g) mapping results after post-processing, configuration I—median filter, window of 7 × 7 pixels and unifying five neighbouring images with respect to wavelength λ; (d, h) mapping results after post-processing, configuration II—percentile filter of 20% with windows of size 9 × 9 and 5 × 5 pixels, respectively. [Colour figure can be viewed at wileyonlinelibrary.com]*

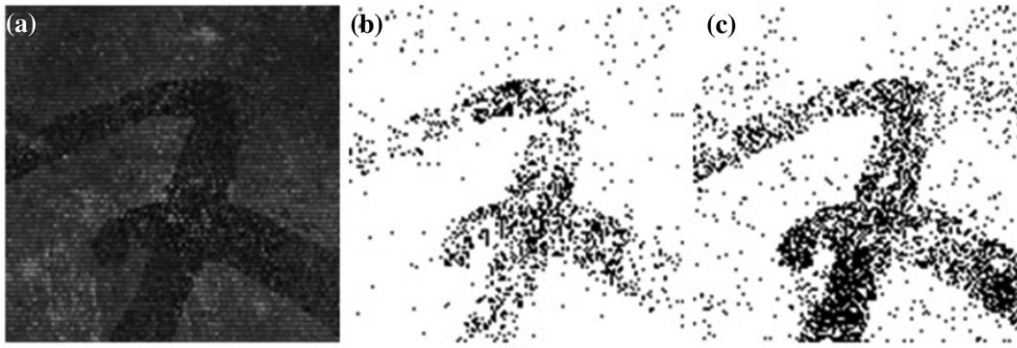

Figure 6 *A comparison of the best PCA, SVM and peak detection results: (a) PCA, the first component; (b) SVM, five-degree polynomial kernel; (c) our peak detection method, I_λ image for ~1460 cm^{-1}.*

the next section). This is as opposed to the SVM, which operates on the whole-spectrum scale and therefore is not readily useful for Raman lines analysis. In other words, both PCA and SVM are general-purpose methods, unaware of the presence of Raman lines. Despite the meaningful PCA and SVM results, our algorithm, specifically designed for the detection of Raman lines, clearly outperforms them.

CONCLUSIONS

The paper deals with the problem of creating automatic objective binary depictions of First Temple period ostraca. As a possible solution, a proof of concept of a new Raman mapping methodology is suggested. The inscription area is sampled via a home-made confocal Raman microscope. Subsequently, the technique overcomes the high fluorescence of the ostraca medium, while circumventing the unattainable ink and clay composition analysis, via the peak detection transformation of the spectra. The detected peaks lead to the creation of a set of macro-scale binary mappings, one for each potential Raman line. The process is concluded with an automatic selection of the best binary images, suggesting the extent to which specific Raman lines are indicative of the ink/clay materials, providing the optimal legibility of the writing. The chosen objective facsimile (or its post-processed variant) can be used in its own right, for any necessary documentation or epigraphic endeavour. It can also supplement and enhance the regular imagery upon registration (see Fig. 5).

It should be emphasized that, despite the challenging fluorescent spectra, and our lack of knowledge of the exact nature of the materials under investigation, it is exceedingly improbable that these results can be achieved at random. The meaningful binary image of the ostraca that we produce is of high statistical significance. Moreover, our results compare favourably with the outcomes of the PCA and SVM techniques.

From a broader perspective, our methodology can be applied not only to ostraca but to other types of ancient inscriptions as well, such as those written on papyri, parchment or paper. We believe that its potential results with non-clay media may be even better due to less significant expected fluorescence. Furthermore, a mapping technique that makes no prior composition assumptions, and that allows for a post-experimental macro-scale material analysis, will make Raman mapping practical, constructive and beneficial in other domains and applications as well.

Several areas of future development and improvement can be proposed:

- While the material analysis up to (and including) image selection and creation is implicit, the collection of I_λ images can be potentially utilized for posterior macro-scale material analysis. This is based upon the fact that the most legible images, either 'positive' or 'negative' (see Fig. 3), represent signals stemming from specific Raman lines.
- The aim of our experiments was to test the plausibility of our approach. Therefore, due to restrictions on laboratory time, we limited ourselves to macro-, yet small-scale scans. Both the quantity and the scale of the experiments can be broadened (e.g., mapping ostraca with other types of ink).
- The output of the peak detection transform may be dependent upon the parameters W and N, which can be optimized automatically.
- The results obtained by a red (671 nm) laser were superior to the results of a green (532 nm) laser. A move to IR lasers may be advisable and ought to be tested. This can also further reduce the potential damage to the ink.
- Currently, the mappings, and their analysis, take 27–48 h for a single character. In the setting of Iron Age inscriptions, this time investment may be valuable enough, since due to the scarcity of epigraphic data from this period, and the shortness of the inscriptions, the identification of a single sign may affect the understanding and interpretation of a word, sentence and even of an entire inscription (Sober *et al*. 2014; Faigenbaum *et al*. 2015; Faigenbaum-Golovin *et al*. 2015, 2017; Mendel-Geberovich *et al*. 2017). Nevertheless, the mapping process can be *substantially* accelerated and streamlined by better auto-focus facilities, or an acoustic optic modulation approach for wide-field parallel observation (Schlücker *et al*. 2003).

ACKNOWLEDGEMENTS

The research reported here received initial funding from the Israel Science Foundation—F.I.R.S.T. (Bikura) Individual Grant no. 644/08, as well as the Israel Science Foundation Grant no. 1457/13. The research was also funded by the European Research Council under the European Community's Seventh Framework Programme (FP7/2007-2013)/ERC grant agreement no. 229418, and by an Early Israel grant (New Horizons project), Tel Aviv University. This study was also supported by a generous donation from Mr Jacques Chahine, made through the French Friends of Tel Aviv University. Arie Shaus is grateful to the Azrieli Foundation for the award of an Azrieli Fellowship. We would also like to acknowledge the indispensable assistance of the late Professor Itzhak Beit-Arieh; as well as the kind help of Ms Sivan Einhorn, Dr Shirly Ben-Dor Evian, Mrs Liora Freud, Mrs Shira Faigenbaum-Golovin and Mrs Myrna Pollak. We would like to thank the editor and anonymous reviewers for their constructive remarks.

REFERENCES

Beit-Arieh, I., 2007, *Horvat 'Uza and Horvat Radum: two fortresses in the biblical Negev*, Tel Aviv University Monograph Series, Vol. **25**, Sonia and Marco Nadler Institute of Archaeology, Tel Aviv.

Cortes, C., and Vapnik, V. N., 1995, Support-vector networks, *Machine Learning*, **20**, 273–97.

Faigenbaum, S., Shaus, A., Sober, B., Turkel, E., and Piasetzky, E., 2013, Evaluating glyph binarizations based on their properties, in Proceedings of 13th ACM Symposium on Document Engineering (DocEng2013), Florence, Italy, 127–30.

Faigenbaum, S., Sober, B., Moinester, M., Piasetzky, E., and Bearman, G., 2015, Multispectral imaging of Tel Malhata ostraca, in *Tel Malhata: a central city in the biblical Negev* (eds. I. Beit-Arieh and L. Freud), 510–13, Vol. **I**, Emery and Claire Yass Publications in Archaeology, Tel Aviv.

Faigenbaum, S., Sober, B., Shaus, A., Moinester, M., Piasetzky, E., Bearman, G., Cordonsky, M., and Finkelstein, I., 2012, Multispectral images of ostraca: acquisition and analysis, *Journal of Archaeological Science*, **39**(12), 3581–90.

Faigenbaum-Golovin, S., Mendel-Geberovich, A., Shaus, A., Sober, B., Cordonsky, M., Levin, D., Moinester, M., Sass, B., Turkel, E., Piasetzky, E., and Finkelstein, I., 2017, Multispectral imaging reveals biblical-period inscription unnoticed for half a century, *PLoS One*, **12**(6), e0178400.

Faigenbaum-Golovin, S., Rollston, C. A., Piasetzky, E., Sober, B., and Finkelstein, I., 2015, The Ophel (Jerusalem) ostracon in light of new multispectral images, *Semitica*, **57**, 113–37.

Faigenbaum-Golovin, S., Shaus, A., Sober, B., Levin, D., Na'aman, N., Sass, B., Turkel, E., Piasetzky, E., and Finkelstein, I., 2016, Algorithmic handwriting analysis of Judah's military correspondence sheds light on composition of biblical texts, *Proceedings of the National Academy of Sciences*, **113**(17), 4664–9.

Gierlinger, N., Keplinger, T., and Harrington, M., 2012, Imaging of plant cell walls by confocal Raman microscopy, *Nature Protocols*, **7**(9), 1694–708.

Gopher, Z., 1981, The composition of the ink and attempts at strengthening the script, in *Arad inscriptions* (ed. Y. Aharoni), Vol. **180**, The Israel Exploration Society, Jerusalem.

Ioffe, Z., Shamai, T., Ophir, A., Noy, G., Yutsis, I., Kfir, K., Cheshnovsky, O., and Selzer, Y., 2008, Detection of heating in current-carrying molecular junctions by Raman scattering, *Nature Nanotechnology*, **3**(12), 727–32.

Lewis, A., 1937, The Lachish letters and the use of iron inks in antiquity, *Nature*, **139**, 470.

Lewis, A., 1938, in *The Lachish letters* (ed. H. Torczyner), 188–97, Oxford University Press, London.

Mendel-Geberovich, A., Shaus, A., Faigenbaum-Golovin, S., Sober, B., Cordonsky, M., Piasetzky, E., and Finkelstein, I., 2017, A brand new old inscription: Arad ostracon 16 rediscovered via multispectral imaging, *Bulletin of the American Schools of Oriental Research*, **378**, 113–25.

Meyer, D., Dimitriadou, E., Hornik, K., Weingessel, A., and Leisch, F., 2015, SVM implementation in the E1071 library, http://cran.r-project.org/web/packages/e1071/index.html (accessed 16 June 2018).

Nir-El, Y., Goren, Y., Piasetzky, E., Moinester, M., and Sober, B., 2015, X-ray fluorescence (XRF) measurements of red ink on a Tel Malhata ostracon, in *Tel Malhata: a central city in the biblical Negev* (eds. I. Beit-Arieh and L. Freud), 507–9, Tel Aviv University Monograph Series, Vol. **32**, Sonia and Marco Nadler Institute of Archaeology, Tel Aviv.

R Development Core Team, 2008, R: A language and environment for statistical computing, R Foundation for Statistical Computing, Vienna, http://www.R-project.org (accessed 16 June 2018).

Ricciardi, P., 2008, Raman spectroscopy for the non destructive characterization of ancient pottery, porcelains and mosaic glasses, 39–66, Ph.D. dissertation, Università degli studi di Firenze, Florence.

Schlücker, S., Schaeberle, M. D., Huffman, S. W., and Levin, I. W., 2003, Raman microspectroscopy: a comparison of point, line, and wide-field imaging methodologies, *Analytical Chemistry*, **75**(16), 4312–8.

Shaus, A., Finkelstein, I., and Piasetzky, E., 2010, Avoiding the eye of the beholder: automated ostraca facsimile evaluation, *Maarav*, **17**(1), 7–20.

Shaus, A., Sober, B., Faigenbaum-Golovin, S., Mendel-Geberovich, A., Piasetzky, E., and Turkel, E., 2016, Facsimile creation: review of algorithmic approaches, in *Alphabets, texts and artefacts in the ancient Near East, studies presented to Benjamin Sass* (eds. I. Finkelstein, C. Robin, and T. Römer), 474–88, Van Dieren, Paris.

Shaus, A., Sober, B., Turkel, E., and Piasetzky, E., 2013, Improving binarization via sparse methods, in Proceedings of 16th International Graphonomics Society Conference (IGS 2013), Nara, Japan, 163–6.

Shaus, A., and Turkel, E., 2016, Chan-Vese revisited: relation to Otsu's method and a parameter-free non-PDE solution via morphological framework, in *Advances in Visual Computing, Proceedings of the 12th International Symposium on Visual Computing (ISVC 2016)* (eds. G. Bebis, R. Boyle, B. Parvin, D. Koracin, F. Porikli, S. Skaff, A. Entezari, J. Min, D. Iwai, A. Sadagic, C. Scheidegger, and T. Isenberg), 203–12, Vol. **I**, Springer International, Cham.

Shaus, A., and Turkel, E., 2017, Towards letter shape prior and paleographic tables estimation in Hebrew First Temple period ostraca, in Proceedings of the 4th International Workshop on Historical Document Imaging and Processing (HIP 2017), Kyoto, Japan, 13–18.

Shaus, A., Turkel, E., and Piasetzky, E., 2012a, Quality evaluation of facsimiles of Hebrew First Temple Period inscriptions, in Proceedings of the 10th IAPR International Workshop on Document Analysis Systems (DAS 2012), Gold Coast, Australia, 170–4.

Shaus, A., Turkel, E., and Piasetzky, E., 2012b, Binarization of First Temple period inscriptions—performance of existing algorithms and a new registration based scheme, in Proceedings of the 13th International Conference on Frontiers in Handwriting Recognition (ICFHR2012), Bari, Italy, 645–50.

Sober, B., Faigenbaum, S., Beit-Arieh, I., Finkelstein, I., Moinester, M., Piasetzky, E., and Shaus, A., 2014, Enhancement of ostraca reading: three test cases of multispectral imaging, *Palestine Exploration Quarterly*, **146**(3), 185–97.

Tzang, O., Kfir, K., Flaxer, E., Cheshnovsky, O., and Einav, S., 2011, Detection of microcalcification in tissue by Raman spectroscopy, *Cardiovascular Engineering and Technology*, **2**(3), 228–33.

Appendix A.

DAMAGE ASSESSMENT EXPERIMENTS

As any kind of damage to ancient inscriptions is unacceptable, two sets of experiments were performed in order to check the effect of laser on the ostraca's ink. The experiments aimed at establishing the safe energy levels to be used with the inscriptions. The first set aimed at damaging the inscription, while the second aimed at finding a level with no detectable damage. The results of the experiments were taken into consideration upon performing macro-scale mappings (see the Results section).

Within the destruction experiments, Raman measurements were taken by a home-built system described in the Experimental section (for additional details, see Ioffe *et al*. 2008). The energy increase factors (EIFs) were calculated with respect to the macro-scale setting eventually used (see the Results section); that is, a 671 nm laser beam with a diameter of ~30 μm, an effective power on the samples of ~5 mW, no pixel overlaps and a total exposure time per pixel of ~10 s. For example, using a 532 nm laser (i.e., higher energy levels for the destruction experiment), a smaller beam diameter of 0.5 μm, an effective power of 1.25 mW, a step size of 0.25 μm (pixels overlapping by half) and 60 s exposure at each pixel, the EIF is calculated as follows:

$$EIF = \frac{1/532}{1/671} \times \frac{\pi(30/2)^2}{\pi(0.5/2)^2} \times \frac{1.25}{5} \times \frac{1}{0.5} \times \frac{60}{10} \approx 13\,621.8.$$

In order to assess the damage, two digital RGB images *prior to* and *following* the experiment were obtained. A difference image was produced and analysed in its R, G and B bands.

The settings and the results of the two sets of experiments are detailed in Table S1. The nominal settings of the final device can be seen in the last row. The results show that no damage is present even with $EIF \approx 12.6$ (i.e., power levels ~12.6 times higher than in the final device), with certain damage to the artefact starting with $EIF \approx 56.8$. Representative image differences can be seen in Figures S2 and S3, showing a presence and absence of damage for $EIF \approx 56.8$ and $EIF \approx 12.6$, respectively.

SUPPORTING INFORMATION

Additional supporting information may be found online in the Supporting Information section at the end of the article.

Figure S1. The Confocal Raman Microscope: (A) A sketch of the device, comprised of a 671 nm laser, lens system, beamsplitter (BS), Raman notch filter (NF), a spectrograph, an auto-focus mechanism based on a digital camera, and a 3-D scanning table; (B) A photograph of the laboratory setup.

Figure S2. An example of damage induced by the laser, experiment A/4 (EIF = 56.8): (A) prior to the experiment; (B) following the experiment; (C) difference RGB image; (D) R band difference image; (E) G band difference image; (F) B band difference image.

Figure S3. An example of lack of damage induced by the laser, experiment B/3 (EIF = 3.8): (A) prior to the experiment; (B) following the experiment; (C) difference RGB image; (D) R band difference image; (E) G band difference image; (F) B band difference image.

Table S1. Damage experiments details, detailing the EIF (Energy Increase Factors) with respect to the final setting.